2013

On the Use of Rau's Reciprocity to Deduce External Radiative Efficiency in Solar Cells

Xufeng Wang
Purdue University, wang159.purdue.1@gmail.com

Mark S. Lundstrom
Purdue University, lundstro@purdue.edu

On the Use of Rau's Reciprocity to Deduce External Radiative Efficiency in Solar Cells

Xufeng Wang, *Student Member, IEEE,* and Mark Lundstrom*, Fellow, IEEE*

Abstract—**Rau's reciprocity relation has been used to deduce the external radiative efficiency of a wide variety of solar cells using just standard solar cell measurements, but it is based on a number of assumptions, some of which may not be valid for typical thin-film solar cells. In this paper, we use rigorous optical simulations coupled with carrier transport simulations to examine some common thin film solar cells. The results provide guidance on when the Rau relation can be used, why it can fail, and on the magnitude of the errors that can be expected in practice.**

Index Terms—**Photovoltaic cells, thin film devices, electroluminescence (EL), photoluminescence (PL).**

I. INTRODUCTION

THE radiative emission of a solar cell can be a good indicator of its intrinsic quality [1-4]. The external radiative efficiency (ERE) of a solar cell at its open-circuit voltage (V_{OC}) can be defined, as suggested by Green [5], as

$$ERE \equiv \frac{q\phi_{emit}}{J_{dark}(V_{OC})},\qquad(1)$$

where ϕ_{emit} is the total photon flux emitted from the cell and $J_{dark}(V_{OC})$ is the dark current at the V_{OC}. The emitted photon flux can be measured [6-10], but it is not a standard part of solar cell characterization. Given the importance of ERE as a measure of solar cell performance, it would be highly desirable to deduce it from standard solar cell characterization measurements.

To address this need, Rau has proposed a surprisingly simple formula that links a solar cell's ERE with its V_{OC}, short circuit current (J_{SC}), and external quantum efficiency (EQE) as [11]

$$ERE = \frac{\exp(qV_{OC}/kT)\int_0^\infty \phi_B(E)EQE(E)dE}{J_{SC}}\qquad(2)$$

$$\phi_B(E) = \frac{2\pi q}{h^3 c^2}\frac{E^2}{\exp(E/kT)-1},$$

where ϕ_B is the Planck's formula, q is the elementary charge, c is the speed of light, h is Planck's constant, k is Boltzmann's constant, T is the temperature of the cell, and E is the photon energy. In several subsequent works, Rau and others expanded the connection to both photoluminescence (PL) and electroluminescence (EL) [12], and applied (2) to different types of solar cells including CIGS [13]. Recently, Green has applied (2) to a comprehensive set of solar cells ranging from standard c-Si solar cells to organic solar cells [5]. The ERE values deduced from (2) showed reasonable agreement with independently measured ERE values or with expectations in cases for which no measured data was available.

The Rau reciprocity relation (RRR), (2), is based on several assumptions including the validity of the Donolato theorem [14] and superposition [11]. Derived from the principle of detailed balance, the Donolato theorem is a reciprocity relation that states the current collected by the junction surface, S_j, in the presence of a unit point source of carriers at location r is the same as the excess minority-carrier density at r due to a unit carrier density injected on S_j. The superposition principle states that the illuminated IV characteristics of a solar cell $J_{light}(V)$ is composed of the voltage dependent dark injection current $J_{dark}(V)$ and the short circuit current under illumination J_{SC}

$$J_{light}(V) = J_{dark}(V) - J_{SC}.\qquad(3)$$

The work so far has been analytical, starting from these assumptions. In order to test the validity of (2) and understand the conditions under which it may break down, a comprehensive numerical study is needed. In this paper, we perform such a study for some common types of thin film solar cells using an established optical/electrical numerical simulator, ADEPT 2.0 [15]. The results provide insights into the validity of (2).

The paper is organized as follows. Our thermodynamically self-consistent electrical-optical model has been described previously [16]; it is briefly reviewed in Sec. II. In Sec. II, we also define three model structures: i) a thin-film GaAs cell for which we expect the RRR to hold, ii) a CIGS cell for which superposition fails due to the presence of charged traps, and

iii) a CdTe cell for which superposition fails due to the presence of a Schottky barrier at the back contact. In Sec. III, we use numerical simulations to extract the ERE of each of these cells and then compare the results to the ERE deduced from (2). Section IV is a discussion of the results and the conditions under which (2) can fail. We conclude in Sec. V with some general guidelines for using (2) in solar cell analysis.

II. APPROACH

A. Self-consistent Optical Module with the Semiconductor Equations

Since the ERE and the RRR involve both optical (generation, emission, etc.) and electrical aspects (recombination, drift and diffusion transport, etc.), the numerical framework used to study this problem must be overall self-consistent. In this study, we use an enhanced version of ADEPT 2.0, which solves the semiconductor device equations. ADEPT 2.0 is a 1D self-consistent solar cell simulator capable of simulating layered structures. The simulator is well calibrated and is numerically sound. The enhanced version includes photon recycling based on an approach similar to that of Durbin [17]. The details of this implementation are described in [16]. For this work, ADEPT 2.0 has been further upgraded to track the angle and spatially resolved radiative photon emission at the front and back of the solar cell.

B. Model Structures

In this study, we focus on three types of thin film solar cells: GaAs, CIGS, and CdTe. GaAs thin film solar cells currently have the highest reported efficiency (28.8%) for single junction solar cells under 1-sun conditions [18]. The extraordinary intrinsic quality of GaAs double heterostructures gives these cells a very high Shockley-Read-Hall (SRH) lifetime and low surface recombination, and as a result, radiative emission from such cell can be very high [19]. Thus, it can serve as a benchmarking structure where intrinsic radiative emission dominates.

CIGS solar cells can also reach high efficiencies (above 20%) [18]. Unlike the GaAs cells, they display a nonsuperposition behavior—their illuminated and dark IVs cross-over slightly beyond V_{OC} [20]. In addition, the SRH lifetime is low - on the order of nanoseconds due to grain boundaries and bulk defects [21]. As a result, the external radiative efficiency is low in CIGS devices [13]. Compared to GaAs solar cells, which operate as near-ideal PN junction diodes, CIGS solar cells provide us with an opportunity to examine a cell for which superposition fails and nonradiative recombination dominates.

The third solar cell to be examined is a CdTe cell, which also achieve high efficiency but can display a nonsuperposition behavior due to a hole-blocking Schottky barrier at the back contact [22][23]. The methods used to investigate the three types of solar cells we chose in this study can be extended to other types of solar cells.
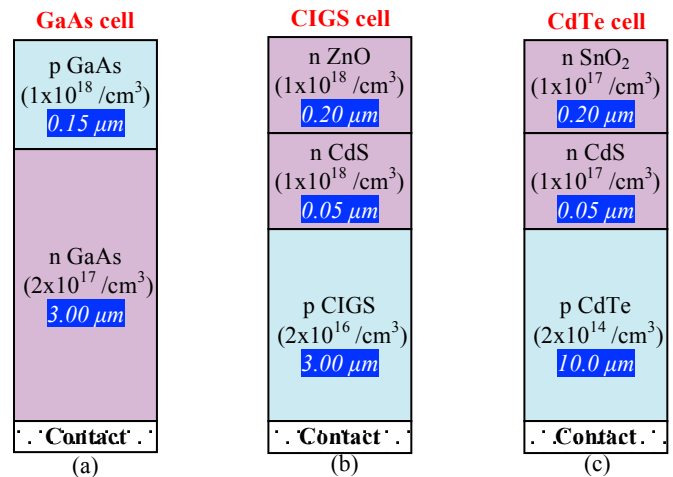

Fig. 1   (a) Baseline single junction GaAs thin film solar cell with reflective back contact. (b) Baseline CIGS solar cell modeled after Gloeckler [25]. (c) Baseline CdTe solar cell modeled after Demtsu [22].

Fig. 1 illustrates the device structures for the GaAs, CIGS, and CdTe solar cells. The model GaAs cell is a simplified version of the structure studied in [16]. Since we do not explicitly simulate the AlGaAs layers passivating the GaAs, an effective surface recombination velocity of 100 cm/s for both top and bottom surfaces are used. Except for the doping density, parameters are identical for both p-type emitter and n-type base. Bandgap reduction due to heavy doping is not included in this study. As discussed in [24], the Roosbroeck-Shockley equation is used to relate the radiative recombination coefficient, B, to the GaAs absorption coefficient. The GaAs absorption coefficients are from experimental data by Lush [26]. A high mirror reflectivity (95%) is used as suggested in [31] as a critical requirement toward high photon recycling and thus high solar cell efficiency.

The baseline CIGS cell structure and material parameters are modeled after Gloeckler [25]. Instead of specifying lifetime, the defect density model is used for SRH recombination with the trap density, energy distribution and capture cross sections specified. We use a Gaussian distribution of defects centered at mid-gap. The conduction band offset at the heterojunction interface between the CdS and CIGS layers is set to 0.3 eV. Radiative emission from the ZnO and CdS layers is minimal because these layers are very thin and have high bandgaps compared to CIGS. Thus, we set the indices of refraction for all layers to be the same as GaAs (3.3) to make later comparisons easier to comprehend. In this study, the specific values of refractive index for each semiconductor layer have minor impact on the results. The refractive index is only used to calculate the escape cone at front surface. Since the ERE values from both RRR and direct computation are calculated through the same optical module, the choice of refractive indices equally affect both calculations. The absorption coefficients for the three layers are taken from [25] and [27].

The CdTe solar cell is modeled after [22]. It is very similar to the CIGS cell except for a lighter base doping (2×10^{14} /cm^3) and a hole-blocking Schottky barrier at the back contact. In this study, we vary the Schottky barrier height to investigate different degree of nonsuperposition. For both CIGS and CdTe solar cells, the back contacts are made from molybdenum with 80% reflectivity [25].

Important material parameters for the baseline GaAs, CIGS, and CdTe cells are summarized in Table 1.

GaAs emitter/base			(a)
Bandgap	1.414 eV	Index n	3.3
Mobility (e)	250 cm^2/V-s	Mobility (h)	500 cm^2/V-s
SRH lifetime	1 μs	Auger coeff.	7×10^{-30} cm^6/s
Surface rec. velocity	100 cm/s (front, rear)	Backside mirror refl.	95%

CdS n+ emitter			(b)
Bandgap	2.4 eV	Index n	3.3
N_{AG}	10^{18} /cm^3	E_D	mid-gap
W_G	0.1 eV	σ_e	10^{-17} cm^2
		σ_h	10^{-12} cm^2
CIGS p-type base			
Bandgap	1.15 eV	Index n	3.3
Mobility (e)	100 cm^2/V-s	Mobility (h)	25 cm^2/V-s
N_{DG}	10^{14} /cm^3	E_D	mid-gap
W_G	0.1 eV	σ_e	5×10^{-13} cm^2
		σ_h	10^{-15} cm^2
Surface rec. velocity	10^7 cm/s (front, rear)	Backside mirror refl.	80%

CdTe p-type base			(c)
Bandgap	1.5 eV	Index n	3.3
Mobility (e)	320 cm^2/V-s	Mobility (h)	40 cm^2/V-s
SRH lifetime	1 ns	Backside mirror refl.	80%

Table 1. Important device parameters for (a) the baseline solar cells, (b) the baseline CIGS solar cell, and (c) the baseline CdTe solar cell. Parameters: donor-like (acceptor-like) defect density N_{DG} (N_{AG}); donor-like (acceptor-like) defect peak energy E_D (E_A); trap Gaussian distribution width W_G; and capture cross-section σ.

III. RESULTS

A. GaAs Solar Cell

As discussed in [11], the validity of the RRR is a sufficient condition for the superposition principle and vice versa. It is therefore helpful to start with a well-behaved pn junction that obeys superposition. We start with a simple GaAs solar cell.

Fig. 2 displays the band diagram and IV characteristics of the GaAs solar cell. The illuminated and dark IV displays no cross-over point so the RRR should hold. As shown in Fig. 3, the ERE values derived from the direct calculation and the RRR agree very well for cases of different mirror reflectivities and carrier lifetimes. Furthermore, not shown here are the results for various base thickness and mobilities, which produce results similar to those in Fig. 3.
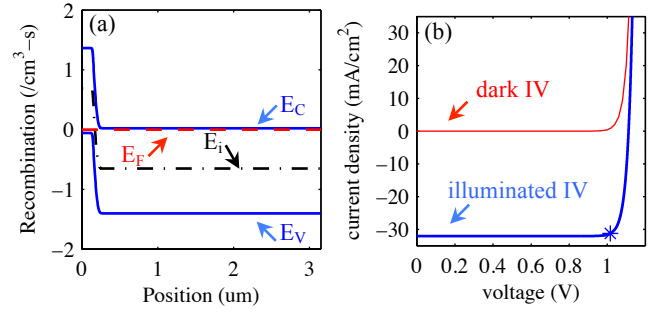

Fig. 2   (a) Equilibrium band diagram for the baseline GaAs solar cell. (b) Illuminated (AM1.5G) and dark IV displaying superposition behavior. The asterisk symbol marks the maximum power point (MPP).
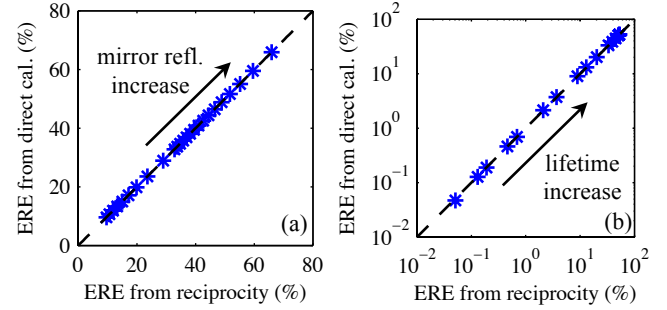

Fig. 3   (a) ERE values derived from the RRR and direct calculation for different mirror reflectivities (0% - 100%). (b) ERE values derived from the RRR and direct calculation for different base minority carrier lifetime (10 ps – 100 μs).

B. CIGS Solar Cell with Trap-induced Nonsuperposition

It is well known that in CIGS solar cells, nonsuperposition behavior can cause the illuminated and dark IVs to cross-over each other. The equilibrium band diagram is shown in Fig. 4a. Compared to the baseline GaAs cell, the CIGS cell has a lighter doping in the base and a larger depletion region (~ 200 nm). In addition, the cell has a heterojunction at the front due to CdS/CIGS interface.
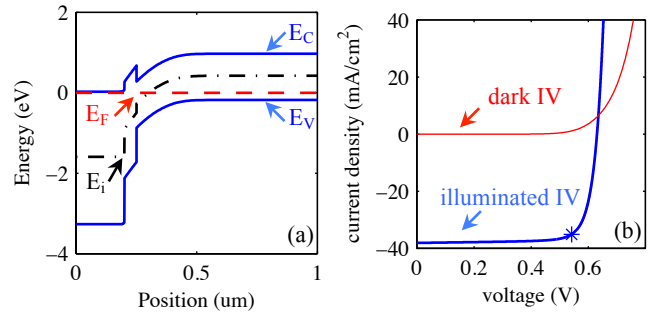

Fig. 4. (a) Equilibrium band diagram for the baseline CIGS solar cell. (b) Illuminated (AM1.5G) and dark IV displaying nonsuperposition behavior. The asterisk symbol marks the maximum power point (MPP).

As pointed out in [25], the conduction band barrier height ΔE_C is a critical factor controlling the cell's nonsuperposition behavior. The CdS layer contains acceptor-like traps that, under illumination when excess amount of electrons and holes

are generated within the n-type CdS emitter, the acceptor-like traps will capture the excess holes and become neutral [32][33]. When the illumination is terminated, the decrease in hole population causes the neutral acceptor-like traps to give up the captured holes and become negatively charge. This as a result causes the bands of CdS shift upward in energy as if a negative bias has been applied to it. In other words, the barrier essentially acts as an illumination-dependent series resistance impeding the flow of electron current in dark. The illuminated and dark IVs showing cross-over are displayed in Fig. 4b.

The RRR is not expected to hold for solar cells that do not display superposition. Fig. 5a shows the comparison for various values of ΔE_C. Clearly, the RRR no longer holds in this case. Moreover, the disagreement between the ERE determined directly and by the RRR increases as the band discontinuity increases and the cross-over becomes more severe as shown in Fig. 5b. More interesting is the fact that the discrepancy between the two approaches has different trends. Increasing conduction band offset decreases the actual ERE but has virtually no effect on the value deduced from the RRR.
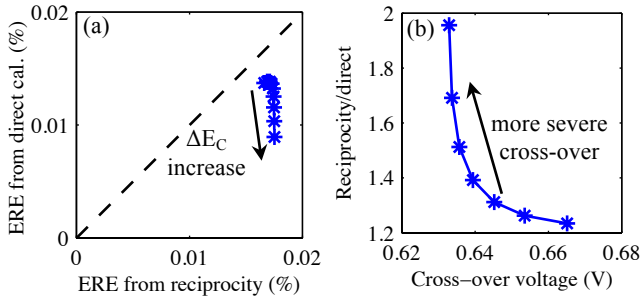
Fig. 5. (a) ERE values derived from the RRR and direct calculation for different ΔE_C (0.1 eV − 0.5 eV, with 0.05 eV increments). (b) Ratio between ERE values from direct computation and the RRR vs. J-V cross-over voltages in Fig. 5a.

The observation can be understood as follows. In dark, the CdS layer acts as a series resistance delaying the turn-on of the diode. The higher the CdS barrier, the lower the current, and the more recombination occurs within the depletion region where non-radiative recombination is more effective than radiative. As a result, the ERE is inversely related to the height of the CdS barrier.

Under illumination, the CdS barrier lowers, and the series resistance it introduced also drops significantly to a point that the cell performance is minimally affected. As a result, the height of the barrier has virtually no effect on the EREs derived from the RRR.

Fig. 6 examines two more cases. As shown in Fig. 6a, increasing the CIGS lifetime increases both the actual ERE and the value deduced from the RRR. Some error occurs when using the RRR, but the trend is the same. Fig. 6b shows a more interesting behavior as the trap density in the CdS is varied. Increasing trap density decreases the actual ERE but has almost no effect on the value deduced from the RRR. This behavior is similar to what was observed for the varying conduction band discontinuity in Fig. 5. Under dark

conditions, with increasing acceptor-like trap concentration in the CdS layer, the CdS barrier height increases and more strongly impedes the electron current. As a result, the actual ERE decreases with increasing trap density. Under illumination, the traps become neutral and have minimal effect in impeding the electron current flow. Thus, the ERE derived from the RRR is unaffected by a change of the trap density.
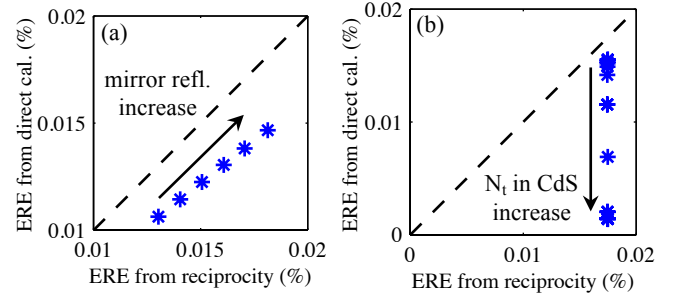
Fig. 6. (a) ERE values derived from the RRR and direct calculation for different mirror reflectivities (0% - 100%, with 20% increments). (b) ERE values derived from the RRR and direct calculation for different trap density (8.5×10^{17}, 9×10^{17}, 1×10^{18}, 1.5×10^{18}, 2×10^{18}, 2.5×10^{18}, and 3×10^{18} /cm^3) in CdS layer. Conduction band offset is set at 0.3 eV and is unaffected by the trap density.

C. CdTe Solar Cell with Backside Schottky Barrier-induced Nonsuperposition

CdTe solar cells with a backside Schottky barrier can display nonsuperposition behavior very much like the CIGS solar cells as displayed in Fig. 7. The situation in a real CdTe solar cell is complicated with the presence of both a Schottky back contact and a valence band offset at the CdS/CdTe interface. As shown in Fig. 8a, the RRR seriously under-estimates the true ERE. This is opposite to what we observed in case of the CIGS cells, indicating that, although both types of cells display nonsuperposition, the mechanisms behind the deviation of the RRR from the true ERE values are different.
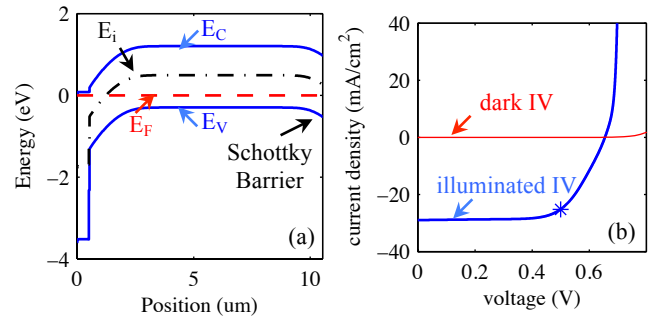
Fig. 7. (a) Equilibrium band diagram for the baseline CdTe solar cell. (b) Illuminated (AM1.5G) and dark IV displaying nonsuperposition behavior. The asterisk symbol marks the maximum power point (MPP).

The reason for the failure of the RRR in case of CdTe cell rests in the conservation of charge. Let us begin with the equilibrium band diagram in Fig. 7a. If the cell is suddenly illuminated, excess electrons and holes are generated. The excess holes have only two routes to exit the structure: 1) by

recombination with electrons, and 2) by escaping through the rear Schottky barrier.

Under short-circuit conditions, the bulk recombination is minimal, so most excess holes escape by the Schottky barrier. To permit this increase in hole current, the bands in the CdTe quasi-neutral region shift downward in energy forward biasing the Schottky barrier. At the same time, the voltage drop across the front pn junction is also reduced. This means less applied voltage is needed to reach the open circuit condition, and thus the V_{OC} is reduced.

The Schottky barrier, however, has little to no impact on J_{SC}. This means that if we compare a CdTe solar cell with a Schottky back contact to one without, we expect to see a reduced V_{OC}, but similar EQE and J_{SC}. As a result, the RRR under-estimates the ERE, and this is exactly what we observe in Fig. 8a. Notice the difference between the two approaches increases exponentially as the Schottky barrier height increases. This occurs because the change in V_{OC} is proportional to the change in barrier height, but the V_{OC} enters the RRR as $\exp(qV_{OC}/kT)$.
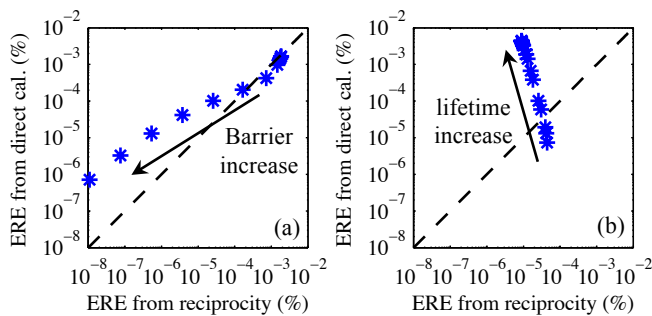

Fig. 8. (a) ERE values derived from the RRR and direct calculation for different Schottky barrier height (0 eV – 0.5 eV, with 0.05 eV increments). (b) ERE values derived from the RRR and direct calculation for different base minority carrier lifetime (10 ps – 100 µs) with a Schottky barrier height of 0.4 eV.

When the CdTe lifetime is varied, the resulting comparison between ERE values from the RRR and direct calculation is intriguing. The increasing ERE from the direct calculation with increasing lifetime is expected since higher non-radiative lifetime permits more radiative emission. The decreasing ERE from the RRR with increasing lifetime is however counter-intuitive and can be explained as follows.

With low carrier lifetime, the majority of the recombination occurs within the bulk. The bulk recombination increases as the cell is biased toward V_{OC}. However, not all of this applied bias drops across the front pn junction. The increased bulk recombination requires an increased supply of holes, which is accomplished by reverse biasing the Schottky barrier. Thus, part of the applied bias in fact goes to reverse biasing the rear Schottky barrier. As a result, the cell with a lower carrier lifetime requires more voltage to be applied to reach open-circuit condition and thus has a higher V_{OC}. This however does not mean a lower lifetime will yield a more efficient solar

cell. The increasing reverse bias on the Schottky barrier as the cell is biased toward V_{OC} acts as an increasing series resistance that severely degrades the fill-factor. As a result of this fill-factor degradation, the cell efficiency decreases with decreasing lifetime, despite the slight increase in V_{OC}. Similar counterintuitive behaviors are also reported in [30] where the rate of photoluminescence decay increases with mobility with the presence of strong surface recombination.

IV. DISCUSSION

From the previous section, we have seen that the most significant factor deviating the ERE calculated using the RRR from its true value is the violation of the superposition principle. In addition, we observe that as the nonsuperposition behavior becomes increasingly severe, the deviation becomes larger.

As Moore et al. pointed out in [28], nonsuperposition in fact can be observed in all types of solar cells due to bias dependent light generation current. As the solar cell is biased toward the built-in voltage, V_{bi}, the built-in electric field reduces, and eventually the light generated carriers will have equal chance to reach both contacts. At this point, the light generated current becomes zero, and the dark and illuminated IVs cross-over. This universal nonsuperposition behavior however is not the cause for the error of the RRR. In fact, in the typical solar cells we investigated in this work, the V_{OC} is far below V_{bi}. At V_{OC}, there is still a significant built-in electric field remain, and the light induced current is not much different from J_{SC}.

The nonsuperposition behavior we observed in the CIGS and CdTe cells is at voltages significantly below V_{bi}. The cause is the dynamic change in their band diagrams under illuminated and dark conditions, instead of the bias dependent light induced current. In the CIGS cell, the CdS layer acts as an illumination-dependent series resistance; and in the CdTe cell, the charge conservation introduces an illumination-dependent bias across the Schottky barrier. This causes the RRR, which assumes identical band diagram under illuminated and dark conditions, to fail.

As a rule of thumb, one should expect the RRR to fail when the cross-over voltage is near V_{OC}. For some situations, the RRR produces errors in the magnitude of the ERE, but displays the correct overall trends (e.g. Figs. 6a and 8a). For other situations, however, the RRR produces trends that are different – even opposite to the correct ERE (e.g. Figs. 6b and 8b).

V. CONCLUSION

The external radiative efficiency of a solar cell can be directly measured or indirectly estimated through the Rau reciprocity relation. In this study, we explored the relation between these two techniques using numerical simulation studies of GaAs, CIGS, and CdTe solar cells. We find that the

Rau reciprocity relation holds very well for cells obeying the superposition principle and fails when the cross-over voltage is near V_{OC}. The cross-over voltage is therefore a helpful indicator for the validity of applying the RRR. When the RRR fails, it produces errors in the estimated ERE. It is surprising, however, that the RRR can produce trends in the estimated ERE as material parameters are varied that are distinctly different and even opposite to those of the actual ERE. When these limitations are understood, the Rau reciprocity relation can be a very useful technique in the characterization of solar cells.

REFERENCES

[1] I. Schnitzer, E. Yablonovitch, C. Caneau, and T. J. Gmitter, "Ultrahigh spontaneous emission quantum efficiency, 99.7% internally and 72% externally, from AlGaAs/GaAs/AlGaAs double heterostructures," Appl. Phys. Lett., vol. 62, pp. 131–133, Jan. 1993.

[2] T. Trupke, J. Zhao, A. Wang, R. Corkish, and M. A. Green, "Very efficient light emission from bulk crystalline silicon," Appl. Phys. Lett., vol. 82, pp. 2996–2998, May 2003.

[3] E. Yablonovitch and T. Gmitter, "Auger recombination in silicon at low carrier densities," Appl. Phys. Lett., vol. 49, pp. 587–589, Sep. 1986.

[4] T. Tiedje, E. Yablonovitch, G. D. Cody, and B. G. Brooks, "Limiting efficiency of Silicon solar cells," IEEE Trans. Electron Devices, vol. ED-31, no. 5, pp. 711–716, May 1984.

[5] M. A. Green, "Radiative efficiency of state-of-the-art photovoltaic cells," Prog. Photovolt: Res. Appl. 20:472−476, 2012

[6] J. E. Cotter, F. W. Chen, T. Trupke, R. A. Bardos, and K. C. Fisher, "Application of photoluminescence characterization to the development and manufacturing of high-efficiency silicon solar cells," Journal of Applied Physics, 100, 11, 2006

[7] J. L. Hernandez, A. Rockett, "Junction electroluminescence of Cu(In,Ga)Se2 devices," Conference Record of the Twenty Fifth IEEE Photovoltaic Specialists Conference, 973-976, 1996.

[8] A. Roos, "Use of an integrating sphere in solar energy research," Solar Energy Materials and Solar Cells, Volume 30, Issue 1, Pages 77–94, June 1993

[9] J. S. Bhosale, "High signal-to-noise Fourier transform spectroscopy with light emitting diode sources," Rev. Sci. Instrum. 82, 093103, 2011

[10] D. Berdebes, J. S. Bhosale, K. Montgomery, X. Wang, A. Ramdas, J. M. Woodall, and M. S. Lundstrom, "Photoluminescence excitation spectroscopy for in-line optical characterization of solar cells," unpublished

[11] U. Rau, "Reciprocity relation between photovoltaic quantum efficiency and electroluminescent emission of solar cells," Physical Review B, 76, 085303, 2007

[12] U. Rau, "Superposition and reciprocity in the electroluminescence and photoluminescence of solar cells," IEEE Journal of Photovoltaics, Vol. 2, No. 2, April 2012

[13] T. Kirchartz, U. Rau, M. Kurth, J. Mattheis, J. H. Werner, "Comparative study of electroluminescence from Cu(In,Ga)Se$_2$ and Si solar cells," Thin Solid Films, 515:6238−6242, 2007

[14] C. Donolato, "A reciprocity theorem for charge collection," Appl. Phys. Lett., 46(3), 1985

[15] J. L. Gray, X. Wang, and X. Sun, "ADEPT 2.0," http://nanohub.org/resources/adeptnpt

[16] X. Wang, M. R. Khan, J. L. Gray, M. A. Alam, and M. S. Lundstrom, "Design of GaAs solar cells operating close to the Shockley-Queisser limit," IEEE J. Photovolt. PP99, 1−8 (2013)

[17] S. M. Durbin, J. L. Gray, R. K. Ahrenkiel, and D. H. Levi, "Numerical modeling of the influence of photon recycling on lifetime measurements," 23rd IEEE PVSC, p. 628, 1993

[18] M. A. Green, K. Emery, Y. Hishikawa, W. Warta, and E. D. Dunlop, "Solar cell efficiency tables (Version 40)," Volume 20, Issue 5, pages 606–614, August 2012

[19] I. Schnitzer, E. Yablonovitch, C. Caneau, and T. J. Gmitter, "Ultrahigh spontaneous emission quantum efficiency, 99.7% internally and 72% externally, from AlGaAs/GaAs/AlGaAs double heterostructures," Appl. Phys. Lett., 62, 2, 1993

[20] M. Gloeckler, C. R. Jenkins, and J. R. Sites, "Explanation of light/dark superposition failure in CIGS solar cells," Mat. Res. Soc. Symp. Proc., 763, 231, 2003

[21] Q. Cao, O. Gunawan, M. Copel, K. B. Reuter, S. Jay Chey, V. R. Deline, and D. B. Mitzi, "Defects in Cu(In,Ga)Se$_2$ chalcopyrite semiconductors: a comparative study of material properties, defect states, and photovoltaic performance," Advanced Energy Materials Volume 1, Issue 5, pages 845–853, October, 2011

[22] S. H. Demtsu, and J. R. Sites, "Effect of back-contact barrier on thin-film CdTe solar cells," Thin Solid Films, Volume 510, Issues 1–2, 3 July 2006, Pages 320-324

[23] A. Niemegeers, and M. Burgelman, "Effects of the Au/CdTe back contact on IV and CV characteristics of Au/CdTe/CdS/TCO solar cells," J. Appl. Phys. 81, 2881 (1997)

[24] W. van Roosbroeck, and W. Shockley, "Photon-radiative recombination of electrons and roles in Germanium," Physical Review 94, 1558, 1954

[25] M. Gloeckler, "Device physics of Cu(In,Ga)Se$_2$ thin-film solar cells," PhD dissertation, 2005

[26] G. B. Lush, "Recombination and absorption in n-type gallium arsenide" PhD dissertation, http://docs.lib.purdue.edu/ dissertations/AAI9301343/

[27] P. D. Paulson, R. W. Birkmire, and W. N. Shafarman, "Optical characterization of CuIn$_{1-x}$Ga$_x$Se2 alloy thin films by spectroscopic ellipsometry," J. Appl. Phys., 94, 879, 2003

[28] J. Moore, C. Hages, S. Dongaonkar, R. Agrawal, and M. Lundstrom, "The Physics of IV Crossover in Thin Film Solar Cells," (Unpublished)

[29] R. F. Pierret, Semiconductor Device Fundamentals, Addison-Wesley, Reading, MA, 1996.

[30] R. K. Ahrenkiel, "Influence of junctions on photoluminescence decay in thinfilm devices," J. Appl. Phys. 62, 2937 (1987)

[31] B. M. Kayes, et al., "27.6% conversion efficiency, a new record for single-junction solar cells under 1 sun illumination," 37th IEEE PVSC, June 2011

[32] M. Burgelman, et al., "Defects in Cu(In, Ga)Se$_2$ semiconductors and their role in the device performance of thin-film solar cells," Prog. Photovoltaics. Res. Appl., 5, p. 121, 1997

[33] A. Kylner, "Effect of impurities in the CdS buffer layer on the performance of the Cu(In, Ga)Se$_2$ thin film solar cell," J. Appl. Phys., 85, p. 6858, 1999
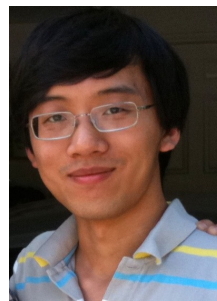
Xufeng Wang (S'08) received B.S. degree in electrical engineering in 2008 and M.S. degree in electrical engineering in 2010, both from Purdue University, West Lafayette, IN. Since 2010, he has been a PhD student conducting research at Network for Photovoltaic Technology (NPT) at Purdue University.

His current research focuses on the electronic transport and optics coupling in high performance thin film solar cells.

Mark S. Lundstrom (S'72–M'74–SM'80–F'94) is the Don and Carol Scifres Distinguished Professor of Electrical and Computer Engineering. His current research interests center on the physics of small electronic devices, particularly nanoscale transistors, on carrier transport in semiconductor devices, and on devices for energy conversion, storage, and conservation.

Dr. Lundstrom is a Fellow of the American Physical Society and the American Association for the Advancement of Science and a member of the U.S. National Academy of Engineering.